

## Relative humidity control for atomic force microscopes

Oleg Stukalov, Chris A. Murray, Amy Jacina, and John R. Dutcher

*Department of Physics, University of Guelph, Ontario N1G 2W1, Canada*

(Received 28 November 2005; accepted 5 February 2006; published online 28 March 2006)

We describe the design and performance of a relative humidity (RH) control chamber for use with atomic force microscopes (AFM) in which the tip is scanned across the stationary sample. The small volume ( $\sim 9 \text{ cm}^3$ ) chamber encloses the sample, the cantilever holder, and a commercial humidity/temperature sensor. The RH is controlled by passing a controlled ratio of dry and humid nitrogen gas across the sample. This unique design prevents exposure of the scanner assembly to humid gas and maintains all of the functionalities of the AFM system with no measurable degradation of its performance. Using this system, the RH at the sample position can be varied between 5% and 95% and controlled to within  $\pm 0.2\%$  during an AFM measurement. To demonstrate the performance of the RH control chamber in imaging and force spectroscopy modes, we have characterized the RH-dependent swelling of small chitosan droplets with diameters of 3–40  $\mu\text{m}$ , and the RH dependence of capillary forces between the AFM tip and a mica surface. © 2006 American Institute of Physics. [DOI: 10.1063/1.2182625]

### I. INTRODUCTION

One of the numerous advantages of atomic force microscopy (AFM) that has allowed this technique to be used in a wide variety of scientific fields is the ability to perform measurements in different environments.<sup>1</sup> *In situ* variation of the relative humidity (RH) of the air surrounding the sample during an AFM measurement allows the user to address a number of issues, e.g., the influence of capillary forces<sup>2,3</sup> on AFM imaging,<sup>4</sup> nanoscale friction and wear,<sup>5,6</sup> adhesion between microparticles and surfaces,<sup>7</sup> conformational changes of single molecules,<sup>8</sup> and changes in mechanical properties and morphology of various materials ranging from natural fibers<sup>9,10</sup> to contact lenses<sup>11</sup> and cement paste.<sup>12</sup>

The choice of method for controlling the RH depends on the design of the AFM used for the measurements. For the case in which the AFM scanning head is compact, the head can be placed within a closed chamber, where the desired RH is maintained,<sup>13</sup> or a smaller chamber can be constructed that encloses only the sample and the cantilever components.<sup>2</sup> The RH value can be adjusted by using water absorbent material, a water evaporative source, or by flowing a mixture of gas with controlled RH past the sample.<sup>14</sup> Ideally the chamber should have a volume which is well sealed and as small as possible for good control of RH. Additionally, exposure of electronic components and optics to high humidity should be avoided especially for higher RH for which condensation of water onto solid surfaces can occur. These considerations are particularly important for AFM designs in which the scanning head is rather large and contains additional electronics and/or a motorized translation stage, such as the Dimension series (Digital Instruments, Veeco Metrology) of AFMs.

Martin *et al.*<sup>15</sup> and Maxwell and Huson<sup>14</sup> reported the design of an environmental chamber for use with Dimension series AFMs. Both designs expose the piezoelectric scanner to high humidity and restrict the translation capabilities of the sample translation stage. Additionally, the design of Ref.

15 is rather complicated and it cannot be simply adapted for use with other AFM systems. In the design of Ref. 14, the chamber is large and poorly sealed such that the RH value near the sample surface is difficult to control.

In the present article we report the design of a simple, small chamber for the control of RH for AFMs in which the tip is scanned across a stationary sample. The RH control chamber has improved performance relative to previous designs. We demonstrate its performance in imaging mode by measuring the RH-dependent swelling of small chitosan droplets, and in force spectroscopy mode by measuring the RH-dependent adhesion forces between the AFM tip and a mica surface.

### II. TECHNICAL DESCRIPTION OF RH CONTROL CHAMBER

In this section, we describe in detail a RH control chamber that was designed for use with a Dimension 3100 AFM, in which the tip is scanned by a piezoelectric tube across a stationary sample. A schematic diagram and a photograph of the chamber are shown in Fig. 1. The chamber consists of four major components: (1) a Delrin (polyoxymethylene) mount for the AFM cantilever holder [Fig. 1(d)], (2) a lucite ring [Fig. 1(f)] onto which is placed (3) a rubber membrane containing a central hole [Fig. 1(e)], and (4) a flat lucite base [Fig. 1(g)]. After the AFM cantilever holder is placed in the Delrin mount, the mount is inserted into the central hole in the rubber membrane. This assembly is then placed onto the piezoelectric scanner of the Dimension AFM head [Fig. 1(a)] using the four-pin connector on the cantilever holder. The AFM head with the attached assembly is then mounted onto the AFM head holder such that the lower surface of the lucite ring is just touching the lucite base of the AFM. Therefore, the ring, the rubber membrane, and the lucite base form a closed, low volume ( $\sim 9 \text{ cm}^3$ ) chamber containing the sample and the cantilever. For force-distance measurements

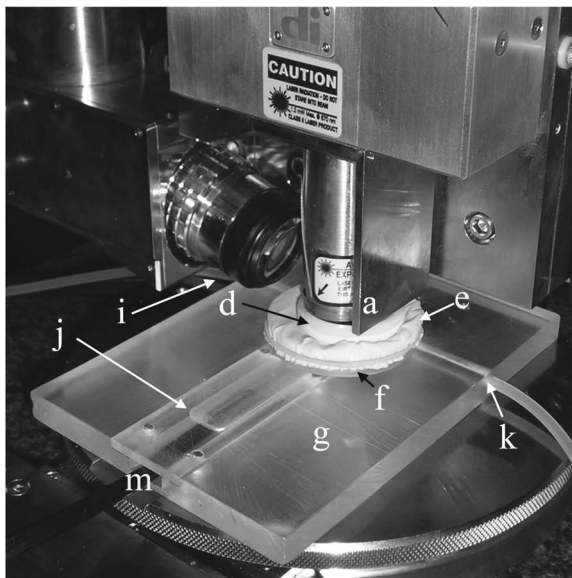
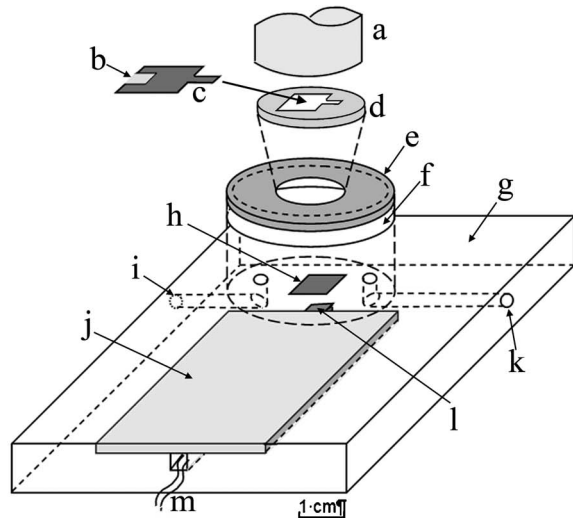


FIG. 1. Schematic diagram of the AFM relative humidity (RH) control chamber (top) and a photograph of the RH control chamber (bottom): (a) lower part of piezoelectric scanner tube, (b) the piece of glass cover slip attached to the four-pin Dimension AFM cantilever holder (c), (d) Delrin mount for standard cantilever holder, (e) circular rubber membrane with hole punched in the center, (f) lucite ring, (g) lucite base, (h) sample, (i) humid gas flow inlet, (j) cover plate, (k) humid gas flow outlet, (l) humidity sensor placed in a groove within the base, and (m) wires from the sensor.

or frictional force measurements for which imaging in tapping mode is not required, it is convenient to replace the Delrin mount with a fluid cell cantilever holder, such as that supplied with the Dimension and Bioscope (Veeco) systems.

### A. Design considerations

For stable imaging under high humidity conditions, it is preferable to use high-frequency tapping mode and therefore one should use the Delrin mount with the standard four-pin cantilever holder that contains a piezoelectric transducer for exciting the oscillations of the cantilever. The fluid cell holder should be used for force-distance measurements or frictional force measurements and when surface imaging using tapping mode is not essential.

The circular Delrin mount [Fig. 1(d)] with an outer diameter of 3 cm contains a central hole that is designed to fit the shape of the standard four-pin Dimension AFM cantilever holder [Fig. 1(c)] and also to allow the laser beam reflected from the end of the cantilever to pass through the holder. To ensure proper sealing at the top of the RH control chamber, a small piece of glass cover slip [Fig. 1(b)] was placed over the hole in the cantilever holder which allows the laser beam to pass. The use of the glass cover slip causes a small reduction in the sum signal of the photodiode and slightly complicates the focusing of the optical microscope on the cantilever due to an undesirable reflection of the incident light of the optical microscope system. The use of a glass cover slip with an antireflection coating would result in less deterioration of the optical system quality. Nevertheless, we have found that the use of an uncoated glass cover slip does not significantly degrade the overall performance of the AFM.

The maximum radius and height of the lucite ring [Fig. 1(f)] are determined by the dimensions of the scanner head and the space available around the scanner head for the particular AFM being used. For the Dimension AFM used in the present study, the radius of the lucite ring should be less than the distance from the center of the piezoelectric scanner assembly to the front of the optical microscope objective and the Dimension AFM head dovetail groove. A ring outer diameter of 4.5 cm was found to be optimal. The ring height is also limited by the close proximity of the objective lens of the AFM and it was chosen to be  $\sim 1$  cm for commonly used thin substrates such as silicon and mica. For thicker samples, the lucite ring height should be increased.

The choice of material, size, and mounting of the rubber membrane are crucial to the present design. We found that the rubber membrane should form a good seal on both the Delrin mount/fluid cell holder [Fig. 1(d)] and the lucite ring while remaining loose between both pieces. For the case of the Delrin mount, the best results were obtained using a rubber membrane that was cut from a thin sheet of latex, whereas using the neck cut from a medium size, helium-grade latex balloon worked best for the case of the fluid cell holder. To check whether the presence of the rubber membrane affected the  $X$ - $Y$  scanning of the AFM, a standard calibration grating with  $10\ \mu\text{m}$  pitch and 200 nm depth and a flat silicon wafer were measured with and without the rubber membrane and lucite ring present. It was observed that the rubber membrane did not affect the  $X$ - $Y$  linearity to within the precision of the measurement, and the measured rms roughness values of the silicon wafer were comparable for both configurations. This indicates that the chamber design does not introduce significant imaging artifacts while preserving the spatial resolution of the AFM.

The lucite base of the RH control chamber is held in place by the vacuum chuck of the AFM system and it serves multiple functions. First, it serves as the base of the closed sample chamber, defining the dimensions of the chamber together with the lucite ring [Fig. 1(f)] and the rubber membrane [Fig. 1(e)]. It also contains inlet and outlet ports [Fig. 1(i) and 1(k), respectively] for gas of controlled RH, and a recessed channel to accommodate a commercial relative

humidity/temperature sensor [SHT75, Sensirion, Zurich, Switzerland, [Fig. 1(l)]]]. The sensor wires [Fig. 1(m)] were placed in the channel and were enclosed by a cover plate [Fig. 1(j)] which was held in place with screws (not shown in Fig. 1), such that movement of the base plate did not displace the sensor relative to the lucite base. The sensor was held in place by silicon sealant, such that only the active end of the humidity sensor chip was exposed to humid gas. The distance between the gas inlet and outlet ports together with the diameter of the lucite ring [Fig. 1(f)] restricts the in-plane size of the sample [Fig. 1(h)]. A sample size of less than 1.5 cm was found to be optimal.

A RH generator which combined flow of gas through a dry nitrogen gas line and a wet nitrogen gas line, for which dry nitrogen was bubbled through a water column,<sup>14</sup> was used to control the RH value of the gas supplied to the RH control chamber. Valves were used to adjust the balance of dry and wet gas from the RH generator, and the flow rate supplied to the RH control chamber was adjusted using a precision valve within the range of 0–250 ml/min. Silicon tubing (I.D.=1.5 mm) was used to connect the RH generator and the inlet port [Fig. 1(i)] of the RH control chamber, and to vent the humid gas from the outlet port [Fig. 1(k)] outside of the acoustic isolation hood of the Dimension AFM. The absence of a leak-tight seal between the lucite ring and base plate permits the base plate to be moved by the translation stage without affecting the performance of the piezoelectric scanner, and allowed us the ability to position the AFM tip over any point on the sample within a lateral range of 1.5 cm × 1.5 cm. At the same time the absence of a seal allows small amounts of humid gas to leak out of the RH chamber. However, because of the small gas flow rates, the change in RH outside the chamber during a single AFM experiment is insignificant. To characterize the difference between the RH value measured by the mounted RH sensor and that at the sample position, a second identical RH sensor was placed at the sample position on the base plate and the RH values measured by both sensors were recorded within the range of 5% < RH < 95%. There was no measurable difference between the RH values measured by the two sensors over the entire range of RH values, showing that the original RH sensor values accurately measured the RH at the sample position.

### III. MATERIALS AND METHODS

#### A. Preparation of chitosan droplets

As a test of the RH control system, we chose to study the swelling of small droplets of chitosan, a biodegradable polysaccharide derived from chitin, which is the second most abundant carbohydrate on earth. Chitosan is used for a wide variety of applications in the food and medical industries due to its abundance and unique properties, such as biocompatibility, biodegradability, and bactericidal actions.<sup>16</sup> Chitosan dissolves in weak acids, which allow its preparation in a variety of geometries including fibers, films, and droplets. The polysaccharide network in chitosan can readily absorb water, which leads to large, measurable changes in its volume.

High molecular weight chitosan (Sigma-Aldrich) with a degree of deacetylation (DA) of 0.85 was dissolved in a 2% w/w solution of acetic acid in nanopure water to produce polymer solutions. Typically a 1% w/w polymer solution was used. The solution was sprayed over small (9 × 9 mm<sup>2</sup>) pieces of a Si wafer for several seconds at 55% RH using an atomizer with a fine nozzle. Drying of the samples under ambient conditions resulted in the formation of isolated chitosan droplets ranging in diameter from several micrometers to hundreds of micrometers. The density and size distribution of the droplets were found to be dependent on the concentration of the chitosan solution, the distance from the spray nozzle to the substrate surface, and the spraying time. These parameters were adjusted to produce chitosan droplets with diameters less than 50 μm and a droplet density of ~1–2 droplets per 100 μm (maximum scan size of the Dimension AFM). The samples were transferred to the RH control chamber for AFM measurements after the droplets had dried.

#### B. AFM measurements

Two different types of AFM measurements were performed to test the performance of the RH control chamber: imaging and force-distance measurements.

AFM images were collected using a Dimension 3100 AFM (Digital Instruments, CA, USA) equipped with Nanoscope IV electronics and a standard piezoelectric scanner with a lateral scan extent of 108 μm. Silicon cantilevers (model OMCL-AC160TS,  $k \approx 42$  N/m,  $f_0 \approx 300$  kHz, Olympus, Japan) were used for the AFM imaging. Typically, a rms amplitude  $A_0 \approx 45$  nm and a setpoint  $S=0.8$  were used. The images were collected with NANOSCOPE V5 software and then analyzed using the FEMTOSCAN ONLINE program (Advanced Technology Center, Moscow State University, Moscow, Russia). The FEMTOSCAN ONLINE program allowed the calculation of the volume  $V$  and the basal diameter  $D_b$  of the chitosan droplets after adjusting the threshold plane for the image, and the height  $h$  of the droplet by using the brightness histogram.<sup>17</sup> The threshold plane was adjusted to be 30 nm above the substrate average level to exclude the rough edges of the droplet from the calculations of the  $V$  and  $D$  parameter values. More accurate results for the calculated parameter values were obtained by first applying a first-order flattening procedure to regions of the image that excluded the droplet area. The radius of curvature  $R_c$  of each droplet was also calculated by fitting two measured height profiles of the droplet, chosen to be at right angles to one another, to the equation of a circle and averaging the results. To obtain the best fit profiles, data that were less than 30 nm from the substrate surface were excluded to eliminate the edges of the droplet from the fitting procedure. In all cases very good fits of the equation of a circle to the measured profile were obtained with  $\chi^2$  value per degree of freedom varying by no more than 5% over the entire range of RH.

The error bars for all droplet parameter values were calculated as the standard deviation in the average values of the parameter values obtained from four AFM images that were collected for the same droplet at each RH value during the same experiment. We found that waiting 15 min after adjusting the RH to the desired value in the RH control chamber

was sufficient to stabilize the volume of the droplets and therefore allowed us to neglect dynamic swelling effects. The RH dependence of the parameter values  $h$ ,  $V$ ,  $D_b$ , and  $R_c$  for a droplet was normalized to the corresponding parameter values of the droplet measured at low RH (typically RH  $\sim 5\%$ ).

Force-distance curves ( $f$ - $d$  curves) were collected using contact mode silicon cantilevers (model CSC38, cantilever B, MikroMasch, Estonia). The cantilevers were cleaned with air plasma at medium rf power (model PC-01, Harrick Plasma, NY) for 15 min. It was not possible to measure  $f$ - $d$  curves immediately following plasma treatment of the cantilevers due to a long-range cantilever deflection that is commonly associated with electrostatic repulsion. Only after keeping the cantilever in the grounded AFM holder for several hours under room conditions were reproducible  $f$ - $d$  curves obtained.  $f$ - $d$  curves at different RH values were collected at different surface locations. This was done to eliminate artifacts due to local surface modification of the AFM tip after collecting multiple  $f$ - $d$  curves on the same spot that can change the local surface geometry and affect subsequent adhesion force measurements. We found that it was sufficient to collect and average ten  $f$ - $d$  curves at each RH value to obtain good reproducibility of the adhesion force calculated from the  $f$ - $d$  data. The zero distance on the  $f$ - $d$  curves was chosen to correspond to the point at which the AFM tip snaps into contact with the surface. The force values were calculated by multiplying the deflection of the cantilever measured in volts by the optical lever sensitivity and force constant of the cantilever. The optical lever sensitivity in nm/V was determined from the slope of the approach portion of the  $f$ - $d$  curves.<sup>1</sup> Force constants of cantilevers were calibrated using the “thermal noise” method.<sup>18</sup> The adhesion force was defined as the force needed to pull the tip out of contact with the surface. The  $f$ - $d$  results were analyzed using NANOSCOPE software (Version 6.12).

The commercial RH sensor used in the present study has a constant absolute accuracy of 1.8% for the range 20%  $< \text{RH} < 80\%$ , so AFM data were collected within this range of RH values. Additional AFM data were collected at RH values that were as low as possible (RH  $\sim 5 \pm 3\%$ ) to determine the dimensions of the dry chitosan droplets.

## IV. RESULTS AND DISCUSSION

### A. AFM imaging

We present AFM data collected for two chitosan droplets with basal diameters  $D_b$  of 2.81  $\mu\text{m}$  (small) and 33.05  $\mu\text{m}$  (large). The chitosan droplets used in the present study have the shape of spherical caps surrounded by radially protruding small fibers and very small droplets, as can be seen in the typical AFM image of the small chitosan droplet shown in Fig. 2(a). The small fibers and small droplets surrounding the droplet form during drying. Figure 2(b) shows the dependence of the volume, height, basal diameter, and radius of curvature of the small droplet on RH. It can be seen from Fig. 2(c) that the droplet basal diameter decreases by  $\sim 2\%$ – $3\%$  with increasing RH. A decrease in basal diameter by  $\sim 1\%$  was also measured with increasing RH for the large

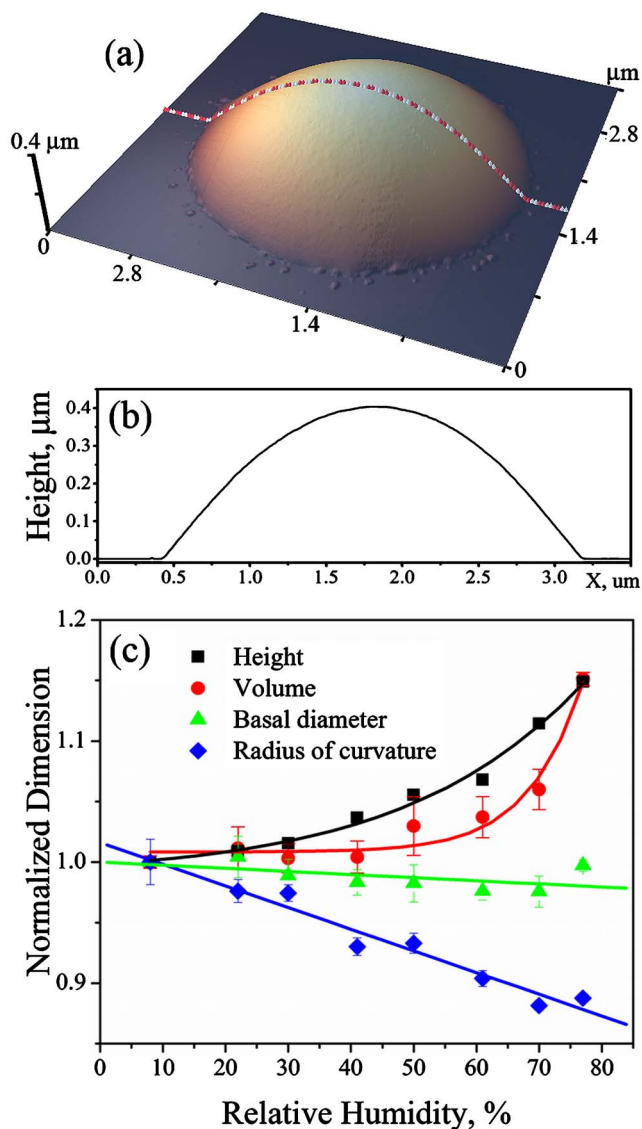


FIG. 2. (Color online) (a) Typical AFM image of the chitosan droplet taken at RH=42%, (b) the height profile corresponding to the dashed line shown on the AFM image and (c) the dependence of its dimensions on RH: height  $h$  (black squares), volume  $V$  (red circles), basal diameter of droplet  $D_b$  measured at 30 nm above substrate surface (green triangles), and radius of curvature  $R_c$  (blue rhombus). The dimensions were normalized to the values measured at RH=8% (height=389.9 nm, volume=1.132  $\mu\text{m}^3$ , diameter =2.81  $\mu\text{m}$ , and radius of curvature=2.52  $\mu\text{m}$ ).

chitosan droplet (data not shown). These small changes in basal diameter (measured at a height of 30 nm above the substrate surface) with RH for the small and large droplets are likely due to small deviations of the droplet shape from a spherical cap following the preparation of the sample towards an elliptical cap with changes in RH that cannot be detected by the present droplet profile fitting procedure. It is most likely that the actual diameter of the droplet in contact with the substrate is independent of RH to within the uncertainty of the measurement due to strong adhesion of the chitosan to the silicon oxide surface. Both the volume and height of the small droplet increases by  $\sim 15\%$  for a RH increase from 8% to 77%, and  $\sim 21\%$  for the large droplet for an RH increase from 5% to 72%. This swelling behavior is similar to that of dextran<sup>19</sup> thin films, for which the thick-

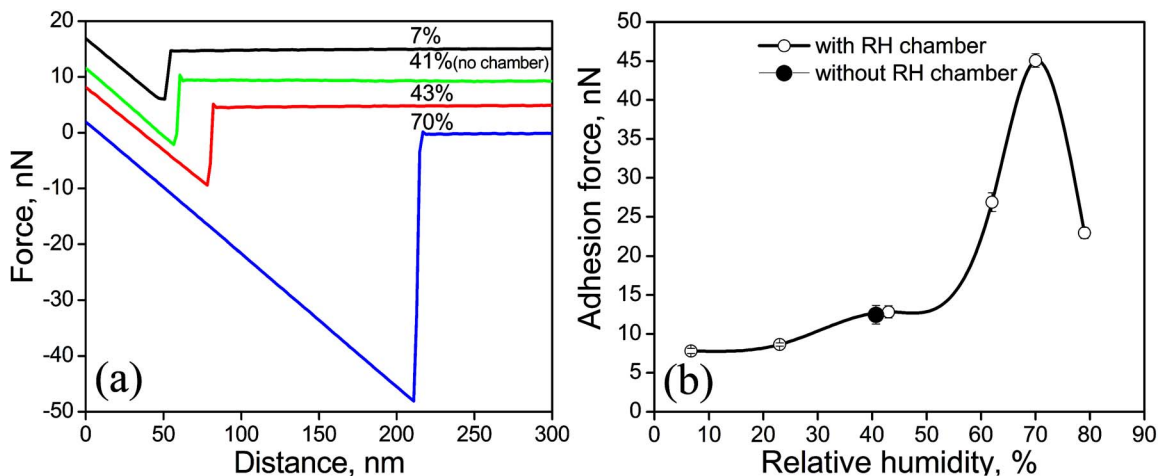


FIG. 3. (Color online) (a) Representative force-distance ( $f$ - $d$ ) curves obtained by retracting a Si cantilever from a freshly-cleaved mica surface at different RH values that are listed next to each curve. (b) Dependence of the adhesion force on relative humidity. The curve is intended only to guide the eye.

ness was observed to increase by a factor of 21.2% (from 166 to 200 nm) with an increase in RH from  $\sim 4\%$  to  $\sim 70\%$ .

The only reported study of RH dependent swelling of chitosan films<sup>20</sup> characterized the swelling of thick (200–400  $\mu\text{m}$ ) films of chitosan, with a DA value that was comparable to that in the present study, by measuring the mass of the films in saturated water vapor (RH=100%). The swelling ratio was reported to be 3.5. Since we were unable to achieve such high RH values with the present RH control chamber design, the data cannot be directly compared.

The decrease of the radius of curvature of the droplet with increasing RH [Fig. 2(b)] is quantitatively consistent with a spherical cap droplet geometry in which the volume increases while the contact area between the droplet and the substrate is fixed. Further improvements of the chitosan droplet spraying procedure are needed to obtain better control over the droplet aspect ratio.

We found that uncertainties in the determination of the droplet volume increased at higher RH values (RH > 70%) due to imaging instabilities, while the determinations of the diameter and the height were less affected at high RH values.

## B. Force-distance curves

Adhesion forces between micrometer- and nanometer-sized objects play a critical role in many areas of science and technology ranging from the processing of fine powders to the design and use of actuators in microelectromechanical systems (MEMS).<sup>21</sup> AFM is one of the major tools for studies of adhesion forces (for recent review see Ref. 22). In ambient conditions, the presence of a thin water layer on each surface gives rise to a capillary effect that produces a significant contribution to adhesion especially for the case when both surfaces are hydrophilic. A number of studies have been devoted to studying capillary effects under controlled RH acting between different surfaces and an AFM tip as a model for a single nanoasperity, in contrast to a multiple nanoasperity contact model for which capillary interactions between colloidal microparticles and a flat surface are considerable.<sup>23</sup>

The hydrophilic/hydrophilic properties of AFM cantilevers and/or surfaces can be altered through plasma and UV-ozone treatment,<sup>24</sup> as well as the deposition of self-assembled monolayers<sup>6</sup> (SAMs) and thin polymer films.<sup>25</sup> Typically, one obtains an insensitivity of adhesion to changes in RH if either the AFM tip or the surface is hydrophobic,<sup>2,6,25–28</sup> whereas adhesion forces are found to be highly sensitive to changes in RH if both the cantilever and the surface are hydrophilic.<sup>2,5,6,23,25,26,28,29</sup> There is disagreement in the literature concerning the RH dependence of the adhesion force involving hydrophilic cantilevers and surfaces. Several authors have reported that the capillary force increases with RH,<sup>23,25,26</sup> with several of these studies reporting a well-defined critical RH value in agreement with the theoretically predicted transition from RH-independent dry adhesion to capillary adhesion at critical RH values varying from  $\sim 10\%$  (Ref. 30) for a mica surface and a  $\text{Si}_3\text{N}_4$  cantilever to  $\sim 60\%$  for the case of a silica surface<sup>23</sup> and a  $\text{Si}_3\text{N}_4$  cantilever. It has also been observed that the adhesive force first increases and then decreases with increasing RH with maxima between 40% and 80% depending on the sample and cantilever tip material.<sup>2,5,6,28,29</sup> To explore this phenomenon further while testing the performance of the RH control chamber, we performed  $f$ - $d$  measurements using hydrophilic Si cantilevers and highly hydrophilic freshly cleaved mica.

We found that Si cantilevers that were stored for a long time in their original Gel-Pak boxes (Gel-Pak, Inc., Hayward, CA) showed no significant dependence of the adhesive force on RH. This is most likely due to silicon oil contamination of the cantilevers resulting from the Gel-Pak cantilever packaging.<sup>31</sup> The situation is different after plasma treatment of the cantilevers which changes the cantilever surface properties from hydrophobic to highly hydrophilic.<sup>24,25</sup> In Figure 3(a) are shown typical  $f$ - $d$  curves collected while retracting the AFM tip from the mica surface for different RH values obtained using the RH control chamber. The dependence of the adhesion force on RH can be clearly seen. Additionally,  $f$ - $d$  curves were collected without the RH control chamber using the standard glass fluid holder and the same tip [see Fig. 3(a)]. A comparison between the data with and

without the RH control chamber shows that the use of the RH control chamber does not produce artifacts in the  $f$ - $d$  curves. In Fig. 3(b) we show the dependence of the adhesion force on RH. The black dot on the graph corresponds to the adhesion measured without the RH control chamber under ambient conditions. This value of the adhesion force is in good agreement with that obtained at the same value of RH using the RH control chamber. We find that the adhesion force increases with increasing RH up to a value of RH  $\sim 70\%$ , and then decreases with further increases in RH, in agreement with the results reported in previous studies.<sup>2,5,6</sup>

## ACKNOWLEDGMENTS

Financial support from the Natural Sciences and Engineering Research Council (NSERC) of Canada and the Province of Ontario (PREA program) is gratefully acknowledged. One of the authors (O.S.) thanks NSERC for a Postdoctoral Fellowship through the NATO Science for Peace program. The authors are also grateful to Steve Wilson for his expert help in the design and construction of the RH control chamber.

- <sup>1</sup>S. N. Magonov and M. H. Wangbo, *Surface Analysis with STM and AFM* (VCH, Weinheim, 1996).
- <sup>2</sup>X. Xiao and L. Qian, *Langmuir* **16**, 8153 (2000).
- <sup>3</sup>L. Zitzler, S. Herminghaus, and F. Mugele, *Phys. Rev. B* **66**, 155436 (2002).
- <sup>4</sup>X. Ji, J. Oh, A. K. Dunker, and K. W. Hipps, *Ultramicroscopy* **72**, 165 (1998).
- <sup>5</sup>J. Hu, X.-D. Xiao, D. F. Ogletree, and M. Salmeron, *Surf. Sci.* **327**, 358 (1995).
- <sup>6</sup>L. Qian, F. Tiang, and X. Xiao, *Tribol. Lett.* **15**, 169 (2003).
- <sup>7</sup>P. Young, R. Price, M. J. Tobyn, M. Buttrum, and F. Dey, *J. Pharm. Sci.* **93**, 753 (2004).
- <sup>8</sup>M. Gallyamov, A. R. Khokhlov, and M. Möller, *Macromol. Rapid Commun.* **26**, 456 (2005).

- <sup>9</sup>R. Resch, R. Ehn, H. Tichy, and G. Friedbacher, *Appl. Phys. A* **A66**, S607 (1998).
- <sup>10</sup>J. M. Maxwell and M. G. Huson, *Micron* **36**, 127 (2005).
- <sup>11</sup>T. S. Koffas, A. Opdahl, C. Marmo, and G. A. Somorjai, *Langmuir* **19**, 3453 (2003).
- <sup>12</sup>T. Yang, B. Keller, and E. Magyari, *J. Phys. D* **35**, L25 (2002).
- <sup>13</sup>P. J. James, J. A. Elliot, J. McMaster, J. M. Newton, A. M. S. Elliot, S. Hanna, and M. J. Miles, *J. Mater. Sci.* **35**, 511 (2000).
- <sup>14</sup>J. M. Maxwell and M. G. Huson, *Rev. Sci. Instrum.* **73**, 3520 (2002).
- <sup>15</sup>J. W. Martin, E. Embree, and M. R. VanLandingham, US Patent No. 6,490,913 (10 December 2002).
- <sup>16</sup>M. N. V. R. Kumar, *React. Funct. Polym.* **46**, 1 (2000).
- <sup>17</sup>J. C. Russ, *The Image Processing Handbook*, 3rd ed. (CRC, Boca Raton, FL, 1998), Chap. 6, p. 371.
- <sup>18</sup>J. L. Hutter and J. Bechhoefer, *Rev. Sci. Instrum.* **64**, 1868 (1993); N. A. Burnham, X. Chen, C. S. Hodges, G. A. Matei, E. J. Thoreson, C. J. Roberts, M. C. Davies, and S. J. B. Tendler, *Nanotechnology* **14**, 1 (2003).
- <sup>19</sup>G. Mathe, A. Albersdörfer, K. R. Neumaier, and E. Sackmann, *Langmuir* **15**, 88726 (1999).
- <sup>20</sup>T. Budtova, N. Belnikovich, L. Kalyuzhnaya, V. Alexeev, S. Bronnikov, S. Veshnebolotskaya, and Z. Zoolshnoev, *J. Appl. Polym. Sci.* **84**, 1114 (2002).
- <sup>21</sup>F. Delrio, M. P. de Boer, J. A. Knapp, E. D. Reedy, P. J. Clews, and M. L. Dunn, *Nat. Mater.* **4**, 629 (2005).
- <sup>22</sup>F. L. Leite and P. S. P. Herrmann, *J. Adhes. Sci. Technol.* **19**, 365 (2005).
- <sup>23</sup>A. A. Feiler, P. Jenkins, and M. W. Rutland, *J. Adhes. Sci. Technol.* **19**, 165 (2005).
- <sup>24</sup>E. Bonaccorso and G. Gillies, *Langmuir* **20**, 11824 (2004).
- <sup>25</sup>H. F. Knapp and A. Stemmer, *Surf. Interface Anal.* **27**, 324 (1999).
- <sup>26</sup>M. Binggeli and C. M. Mate, *Appl. Phys. Lett.* **65**, 415 (1994).
- <sup>27</sup>T. Eastman and D.-M. Zhu, *Langmuir* **12**, 2859 (1996).
- <sup>28</sup>M. He, A. Szuchmacher Blum, D. E. Aston, C. Buenviaje, R. M. Overney, and R. Luginbühl, *J. Chem. Phys.* **114**, 1355 (2001).
- <sup>29</sup>L. Xu, A. Lio, J. Hu, D. F. Ogletree, and M. Salmeron, *J. Phys. Chem. B* **102**, 540 (1998).
- <sup>30</sup>T. Thundat, X. Y. Zheng, G. Y. Chen, and R. J. Warmack, *Surf. Sci. Lett.* **294**, L939 1993; C. E. H. Berger, K. O. van der Werf, R. P. H. Kooyman, B. G. de Grooth, and J. Greve, *Langmuir* **11**, 4188 (1995).
- <sup>31</sup>Y.-S. Lo, N. D. Huefner, W. S. Chan, P. Dryden, B. Hagenhoff, and T. P. Beebe, *Langmuir* **15**, 6522 (1999).